these examples, one or two different physical channels work together; in the present work, we report an organic crystal that simultaneously exhibits bistability in three physical channels: optical, electrical, and magnetic. Moreover, the basic molecular building block can be varied to change the bistability temperature range and the energy gap (which controls the optical and electrical properties).

References and Notes
1. S. A. Wolf *et al.*, *Science* **294**, 1488 (2001).
2. S. Das Sarma, *Am. Sci.* **89**, 516 (2001).
3. R. C. Haddon, *Nature* **256**, 394 (1975).
4. H. Sitzmann *et al.*, *J. Am. Chem. Soc.* **115**, 12003 (1993).
5. P. A. Koutentis *et al.*, *J. Am. Chem. Soc.* **123**, 3864 (2001).
6. R. E. Peierls, *Quantum Theory of Solids* (Clarendon Press, Oxford, 1955).
7. X. Chi *et al.*, *J. Am. Chem. Soc.* **121**, 10395 (1999).
8. M. Ballester, *Acc. Chem. Res.* **18**, 380 (1985).
9. K. Goto *et al.*, *J. Am. Chem. Soc.* **121**, 1619 (1999).
10. X. Chi *et al.*, *J. Am. Chem. Soc.* **123**, 4041 (2001).
11. J. Krober, E. Codjovi, O. Kahn, F. Groliere, C. Jay, *J. Am. Chem. Soc.* **115**, 9810 (1993).
12. O. Kahn, C. J. Martinez, *Science* **279**, 44 (1998).
13. W. Fujita, K. Awaga, *Science* **286**, 261 (1999).
14. K. Nakatani, P. Yu, *Adv. Mater.* **13**, 1411 (2001).
15. Supported by the Office of Basic Energy Sciences, Department of Energy, under grant number DE-FG03-01ER45879.

28 February 2002; accepted 10 April 2002

Binary Asteroids in the Near-Earth Object Population

J. L. Margot,[1]* M. C. Nolan,[2] L. A. M. Benner,[3] S. J. Ostro,[3] R. F. Jurgens,[3] J. D. Giorgini,[3] M. A. Slade,[3] D. B. Campbell[4]
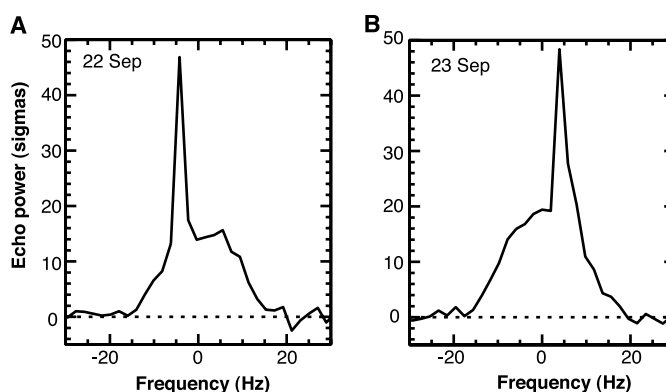
Radar images of near-Earth asteroid 2000 DP107 show that it is composed of an ~800-meter-diameter primary and an ~300-meter-diameter secondary revolving around their common center of mass. The orbital period of 1.755 ± 0.007 days and semimajor axis of 2620 ± 160 meters constrain the total mass of the system to $4.6 \pm 0.5 \times 10^{11}$ kilograms and the bulk density of the primary to 1.7 ± 1.1 grams per cubic centimeter. This system and other binary near-Earth asteroids have spheroidal primaries spinning near the breakup point for strengthless bodies, suggesting that the binaries formed by spin-up and fission, probably as a result of tidal disruption during close planetary encounters. About 16% of near-Earth asteroids larger than 200 meters in diameter may be binary systems.

A small number of asteroids in the main belt between Mars and Jupiter have been shown to have satellites (*1–4*). The presence of a satellite, large or small, allows direct measurements of asteroid masses, which in turn place strong constraints on their density, composition, and internal structure. It raises questions about formation and dynamical evolution and has important implications for our understanding of collisional and disruption processes in the solar system. Speculations about the existence of binary asteroids in the near-Earth population, a dynamically and collisionally distinct class of objects with orbits crossing those of the inner planets, have been made on the basis of the terrestrial impact cratering record, which shows a number of crater pairs (*5*), and on the basis of anomalous lightcurve observations, which show signatures indicative of occultations or eclipses (*6*). Because the lightcurve variations can be due to shape, albedo, spin state, or a combination of those factors, the interpretation of those data sets in terms of binary asteroids has not been universally accepted.

Radar observations provide unambiguous detections of binary asteroids because images at decameter resolution can resolve the individual components. Our observations with the Arecibo and Goldstone radar systems revealed the binary nature of asteroid 2000 DP107 (*7, 8*), which we describe in this paper, and subsequently of asteroids 2000 UG11, 1999 KW4, 1998 ST27, and 2002 BM26 (*9–12*). Asteroid 2000 DP107 was discovered by MIT Lincoln Laboratory's near-Earth asteroid search program (*13*) (LINEAR) on 29 February 2000 at a geocentric distance of 0.6 astronomical units (AU). Its orbit (semimajor axis $a = 1.37$ AU, eccentricity $e = 0.38$, inclination $i = 8.7°$) brought the asteroid within 0.048 AU of Earth, about 19 lunar distances, on 19 September 2000.

Doppler spectra obtained with the 3.5-cm-wavelength Goldstone radar on 22 to 23 September 2000 revealed the presence of a narrowband spike that changed frequency in a manner indicative of an orbiting secondary (Fig. 1). Range-resolved data obtained on 23 September showed separations up to 2 km between the components and suggested that 2000 DP107 was a binary system (*7*). No additional antenna time was available at Goldstone, but a 10-day campaign of observations with the 13-cm-wavelength Arecibo radar on 30 September to 9 October confirmed the existence of a large orbiting secondary.

Most of the Arecibo observing time was devoted to obtaining range-Doppler images, in which radar echoes are resolved along two orthogonal dimensions, range and Doppler shift (*14*). A mosaic of radar images of 2000 DP107 obtained on eight successive days (Fig. 2) shows two well-separated components, with the primary showing the typical signature of a spheroidal object. Estimates of the component sizes can be determined from their range extents. Echo power exceeding three standard deviations of the noise is found in five to six consecutive range bins for the primary and two range bins for the secondary. Assuming that the true diameter of each object is about twice that of the radar-illuminated fraction, which experience with

[1]California Institute of Technology, MC 150-21, Pasadena, CA 91125, USA. [2]National Astronomy and Ionosphere Center, Arecibo, Puerto Rico 00612. [3]Jet Propulsion Laboratory, 4800 Oak Grove Drive, Pasadena, CA 91109, USA. [4]Space Sciences Building, Cornell University, Ithaca, NY 14853, USA.

*To whom correspondence should be addressed. E-mail: margot@gps.caltech.edu

Fig. 1. Goldstone echoes resulting from a monochromatic transmission at 3.5-cm wavelength were spectrally analyzed at 2-Hz resolution and show a narrowband spike superposed on a broadband component. The wide-bandwidth echo is indicative of a rapidly rotating primary object, whereas the narrowband feature, which moves at a rate different from the rotation of the primary, represents power scattered from a smaller and/or slowly spinning secondary. The narrowband echo oscillates between negative and positive frequencies, representing the variations in Doppler shift of an object revolving about the system's center of mass. Data are from 22 September (**A**) and 23 September (**B**).

shape modeling (15) has shown is true if the object is spheroidal (16), we adopt diameters of 800 m and 300 m, for the primary and secondary, respectively. We assign uncertainties to those sizes corresponding to twice our range resolution, i.e., relative uncertainties of 20% for the primary and 50% for the secondary.

The power distribution in the Doppler dimension (Fig. 2) constrains the spin states of the two components (17). The primary extends over 6.9 ± 0.7 Hz, which for an 800-m-diameter object corresponds to a spin period of $3.2 \sin \delta$ hours, where δ is the inclination of the spin axis with respect to the line of sight. This measurement is consistent with a more accurate determination of the spin period (2.77536 ± 0.00024 hours) obtained from lightcurve observations (18). In Arecibo images processed at higher frequency resolution than shown in Fig. 2, the secondary extends on average over an $\sim$0.18-Hz bandwidth, providing an upper bound of $\sim$46 hours on its spin period. The fast rotation of the primary is a common attribute of radar-detected binary NEAs (7–12).

Range-Doppler images obtained at different epochs reveal the co-orbital motion of the primary and secondary, with perceptible motion of the primary around the center-of-mass (COM) of the system. Estimates of the separations between the primary and the secondary were measured along the range and Doppler dimensions in summed images spanning 30 min (19). The

motion of the components during that time interval is close to our image resolution. This resulted in 24 distance and velocity measurements from 8 days of Arecibo imaging data (30 September to 7 October 2000) and 1 day (23 September) of Goldstone data and 15 velocity measurements from spectra obtained at Goldstone (22 to 23 September) and Arecibo (30 September to 9 October).

The relative positions and velocities of the secondary with respect to the primary can be described by the two-body problem of celestial mechanics (20). We modeled the dynamics of the system with seven parameters: orbital period P, semimajor axis a, eccentricity e, three Euler angles defining the orientation of the orbital plane and the pericenter location (Ω, i, ω), and the epoch of pericenter passage T. Aspect changes as Earth and the asteroid moved through space during the course of the radar observations were accounted for. The model was fit to the data in a least-squares sense with 2100 starting values spanning a range of plausible initial conditions. The best-fit solution (reduced $\chi^2 = 0.32$, Table 1) yields an orbital period $P = 1.755 \pm 0.007$ days and a semimajor axis $a = 2620 \pm 160$ m. Our period estimate is consistent with lightcurve brightness attenuations that were reported to occur on time scales of 1.76 ± 0.02 days (18). The similarity of the orbital and spin periods of the secondary suggests that it is locked in synchronous rotation

with the primary, similar to the Earth-Moon system.

The mean sidereal motion $n = 2\pi/P$ and semimajor axis a constrain the system's total mass M_t by Kepler's third law $n^2a^3 = GM_t$, where G is the gravitational constant. Given the period and separation estimated above, the total mass of the system $M_t = 4.6 \pm 0.5 \times 10^{11}$ kg (Fig. 3). The correction to the mass due to a nonuniform gravitational field (21) should not exceed a few percent. Because the primary and the secondary have diameter ratios of $\sim$8:3, their volume and mass ratios, assuming similar densities, are $\sim$20:1. An independent verification of this mass ratio is given by the ratio between a and the amplitude of the motion of the primary around the COM (20). By fitting the ephemeris range residuals from 30 September to 7 October (22), we find that the motion of the primary around the COM has an amplitude of 140 ± 40 m, yielding a mass ratio of $\sim$19:1. Therefore the total mass is a good estimate of the mass of the primary. Our mass estimate, as well as preliminary size and shape estimates and their uncertainties, can be used to derive the density of the primary, $\rho = 1.7 \pm 1.1$ g cm^{-3} (23).

Because the grain density of plausible stony meteorite analogs ranges from 2.4 to 3.8 g cm^{-3} (24), the volume of void space required to match the nominal bulk density of the primary is 29 to 55% of the total volume. This suggests that 2000 DP107 may be a porous, gravitationally bound aggregate. Several asteroids with low bulk density and high porosity have been observed in the main belt of asteroids (2, 3), including the 1.3 g cm^{-3} asteroid 253 Mathilde visited by the NEAR spacecraft (25).

We can derive additional constraints on material properties by examining the tidal evolution of the binary system. A prograde secondary orbiting above the synchronous height (26) undergoes an expansion of its orbit because the tidal torque on the secondary acts to increase the system's orbital angular momentum. The rate of
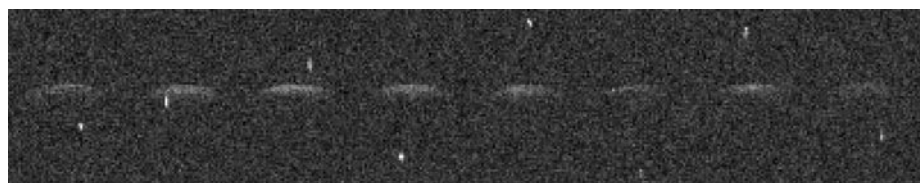

Fig. 2. Mosaic of eight range-Doppler images of binary asteroid 2000 DP107 obtained at Arecibo Observatory from 30 September to 7 October 2000. Each frame is 5.8 km vertically by 12.2 Hz horizontally, with range, or distance from the observer, increasing downward and Doppler, or line-of-sight velocity with respect to the observer, increasing to the right. The resolutions are 75 m in range and 0.24 Hz (15 mm s^{-1}) in Doppler. Rotation and revolution are counterclockwise. A roughly spherical primary is visible, as well as a secondary at different phases of the orbital cycle. In range-Doppler space the secondary appears much smaller than the primary because its spin rate is lower. The actual size ratio is $\sim$8:3. The rotational and orbital motions of the objects during the 1-hour period over which data were accumulated each day lead to perceptible smearing in range-Doppler space.

Table 1. Least-squares parameter estimates, their formal errors, and correlation matrix. Standard errors quoted in the text are three times as large as the formal errors because there may be systematic sources of error. High correlations between the first two Euler angles Ω and i and the parameters P and a illustrate the difficulty in determining the orbital plane orientation from the range-Doppler data (54). High correlation between the argument of pericenter ω and the time of pericenter passage T is expected for this nearly circular orbit. The calendar date corresponding to the Modified Julian Date (MJD) of 51,820.475 is 2000 October 3 11:24 UTC.

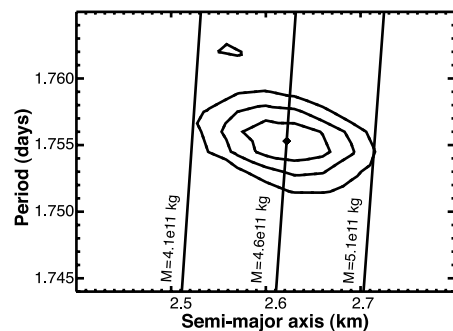| Parameter	Estimate	P	a	T	Ω	i	ω	e
P (days)	1.755 ± 0.0022	1.00						
a (m)	$2,622 \pm 54$	0.41	1.00					
T (MJD)	$51,820.475 \pm 0.30$	0.17	0.22	1.00				
Ω (°)	10 ± 27	0.79	0.84	0.15	1.00			
i (°)	17 ± 7	-0.94	-0.30	-0.03	-0.74	1.00		
ω (°)	7 ± 39	-0.44	-0.41	0.71	-0.59	0.52	1.00	
e	0.010 ± 0.005	0.27	0.22	0.83	0.24	-0.19	0.50	1.00

Fig. 3. χ^2 surface obtained by holding the orbital period and semimajor axis constant while fitting for all other parameters. Contour lines represent the formal 1, 2, and 3σ joint uncertainties in P and a. A diamond indicates the location of the best-fit solution (55). Oblique lines represent loci of constant mass. We adopt mass bounds shown by the outermost oblique lines.

expansion is dependent on material properties through the ratio of Love number k_2 to tidal dissipation factor Q (27). If we assume that the secondary was close to the primary at the time of formation and evolved to its present location, the ratio k_2/Q obtained for evolution during the age of the solar system is 2×10^{-9}. If the binary system formed in near-Earth space rather than in the main belt of asteroids, tidal evolution is restricted to the ~10–million-year (My) median dynamical lifetime of NEAs (28) and yields $k_2/Q = 9 \times 10^{-7}$. In both cases, assuming $Q = 100$, which is typical of silicate-rich bodies (29), yields rigidities for the primary that are less than those of Earth or the Moon. The conclusion that 2000 DP107 is less rigid than typical inner-planet bodies should be regarded with caution because the Q of gravitationally bound aggregates is unknown.

Because our radar data are consistent with synchronous rotation, we used the k_2/Q ratios to determine the tidal despinning time scale, i.e., the time for the secondary to reach synchronous rotation with the primary (30). The necessary time scales are two orders of magnitude smaller than the age of the system, i.e., ~64,000 years if the binary formed in near-Earth space about 10 million years ago (Ma) and ~30 My if the binary formed in the main belt of asteroids about 4600 Ma. Thus, we expect the secondary to be spin-locked to the primary regardless of its formation age. The age of the system can be constrained by examining potential formation mechanisms of binary NEAs, keeping in mind the possibility of formation in the main-belt of asteroids before injection into an Earth-crossing orbit (31). Four possible formation mechanisms are considered.

Formation by capture of two independent asteroids is unlikely due to the low probability of encounters at relative velocities smaller than the components' escape velocity (32). Mutual capture of two fragments after catastrophic disruption of a larger parent body cannot be ruled out, but numerical modeling results indicate that this mechanism favors the formation of contact structures over the formation of true orbiting pairs (33). Capture scenarios cannot easily account for the rapid rotation and sphericity of the primary.

Formation scenarios by way of subcatastrophic impact cratering events have also been proposed (34, 35). The characteristics of satellites formed in this way are small, gravitationally bound aggregates in prograde orbits. To evolve outward tidally, the newly formed companion would have to orbit beyond the synchronous height. Although this requirement places an upper bound on the primary's spin period of about 6 hours (32), it does not require spin rates of ~3 hours, as is observed consistently for NEA binaries identified with radar (7–12) and for additional asteroids showing eclipse or occultation events in lightcurve data (6).

A formation mechanism consistent with the observed rapid spin rates is that of rotational fission (36). In this scenario, an off-center impact delivers enough angular momentum to an asteroid that its spin rate exceeds the breakup point for a strengthless body (37). The asteroid sheds mass, and a companion forms close to the primary and tidally evolves outward. A potential difficulty with this mechanism is that the impact energy required for spin-up is larger than the gravitational binding energy of the object (32), and hence catastrophic disruption outcomes are thought to be more likely.

Finally, we consider rotational spin-up and mass shedding resulting from tidal disruption during a close planetary encounter (38, 39). Monte Carlo (38) and N-body (40) simulations have shown that tidal disruption can result in the formation of binary systems, with secondaries in stable orbits around the progenitor. Analytical (41) and modeling (39) results show that strengthless objects start to shed mass at approach distances within ~0.69 of the Roche limit (42), about 2.5 Earth radii in this case. Because the disruption of interlopers by planetary tides requires an almost total absence of tensile strength (39), binary NEAs formed in this way are expected to be gravitationally bound aggregates. Such strengthless bodies may acquire their spheroidal shapes during the reaccumulation and relaxation after tidal breakup.

The consistent signature of spin rates near the breakup limit suggests that formation of binary NEAs occurs through spin-up and mass shedding, most likely during close planetary encounters (6, 38–40). Tidal evolution considerations strengthen this interpretation because the spin rates of the primaries must have been larger earlier on (43). Calculations show that the primaries of binary systems like 2000 DP107 were indeed spinning at rates faster than the breakup point at the time of formation (44). If the binaries are gravitationally bound aggregates formed in near-Earth space, then they must be young (~10 My).

NEA binaries appear to be common. In a radar survey of ~50 NEAs spanning a wide range of sizes since 1999, we find evidence for five binary systems (7–12). No binaries have been found so far with a primary below a 200-m-diameter threshold (45). The proportion of binary objects among observed NEAs larger than 200 m is about 16%. This number agrees with previous estimates of 15% (38, 40) and 17% (6) from tidal-disruption simulations and lightcurve studies, respectively. This large proportion requires the formation of binaries to be frequent compared with the 10-My dynamical lifetime of NEAs. Asphaug and Benz (39) showed that the probability of mild-to-catastrophic tidal disruptions (i.e., suitable for satellite formation) is about the same as the probability of impact. Although asteroids in the main belt between Mars and Jupiter have been observed in a different size regime (10 to 1000 km as opposed to 0.01 to 5 km for NEAs), the proportion of binaries in that population appears to be on the order of only ~2% (2, 3). Although selection effects cannot be ruled out to explain the discrepancy, we speculate that NEA binaries are formed more readily as a result of repeated close encounters with the inner planets.

References and Notes

1. C. R. Chapman *et al.*, *Nature* **374**, 783 (1995).
2. W. J. Merline *et al.*, in a survey of 300 main-belt asteroids, detected 6 asteroid satellites, 4 of which were previously undiscovered (46–48).
3. J. L. Margot and M. E. Brown, in a survey that has sampled 100 main-belt asteroids so far, discovered satellites to asteroids 87 Sylvia (49) and 22 Kalliope (50).
4. In the rest of this report, we refer to the larger component as "primary," to the smaller component as "secondary" or "satellite," and to both components collectively as "binary asteroid." The terminology is not without its limitations. In many cases it may not be clear which one is the larger or more massive component, and hence which one is the satellite. In other cases, the status of "binary asteroid" would have to be upgraded to "triple asteroid" if another satellite was discovered. The first companion discovered around an asteroid with provisional designation 2000 DP107 receives the provisional designation "S/2000 (2000 DP107) 1" if discovered in the year 2000. A second hypothetical companion discovered in 2002 would receive the provisional designation "S/2002 (2000 DP107) 2."
5. H. J. Melosh, J. A. Stansberry, *Icarus* **94**, 171 (1991).
6. P. Pravec, A. W. Harris, *Icarus* **148**, 12 (2000).
7. S. J. Ostro *et al.*, IAU Circ. No. 7496 (2000).
8. J. L. Margot *et al.*, IAU Circ. No. 7503 (2000).
9. M. C. Nolan *et al.*, IAU Circ. No. 7518 (2000).
10. L. A. M. Benner *et al.*, IAU Circ. No. 7632 (2001).
11. L. A. M. Benner *et al.*, IAU Circ. No. 7730 (2001).
12. M. C. Nolan *et al.*, IAU Circ. No. 7824 (2002).
13. G. Stokes, J. Evans, H. Viggh, F. Shelly, E. Pearce, *Icarus* **148**, 21 (2000).
14. Resolution in range is achieved by transmitting a time-dependent signal and analyzing the radar returns according to their time of arrival, in this case with 0.5-μs time increments corresponding to 75 m in range. Resolution in the Doppler dimension relies on differences in line-of-sight velocities, such as that produced by the apparent rotation of the object as seen by the observer, which imparts a position-dependent Doppler shift to the echoes. Each time history of radar returns corresponding to a specific range resolution bin was Fourier analyzed at 0.24-Hz resolution, which yields a line-of-sight velocity resolution of 15 mm s^{-1}. The resulting two-dimensional array represents power scattered from the target in range-Doppler space.
15. S. Hudson, *Remote Sens. Rev.* **8**, 195 (1993).
16. S. J. Ostro *et al.*, *Meteorit. Planet. Sci.* **36**, 1225 (2001).
17. The spread in Doppler frequency is due to the spin of the asteroids, according to the relation $B = (8\pi R/\lambda P_s) \sin \delta$, where B is the limb-to-limb bandwidth in Hz, R is the target radius, λ is the wavelength of the radar system, P_s is the spin period, and δ is the inclination of the spin axis with respect to the line of sight.
18. P. Pravec, P. Kusnirak, M. Hicks, B. Holliday, B. Warner, IAU Circ. No. 7504 (2000).
19. Because positions could not be reliably estimated from individual imaging runs, data acquired over a half hour were summed to improve the signal-to-noise ratio.
20. C. D. Murray, S. F. Dermott, *Solar System Dynamics* (Cambridge Univ. Press, Cambridge, UK, 1999).
21. Because the gravitational fields of irregular or flattened bodies are not uniform, a correction to Kepler's law is warranted (51):

$$n^2 a^3 = GM_t \left(1 + \frac{3}{2} J_2 \left(\frac{R_p}{a} \right)^2 \right) \qquad (1)$$

where J_2 is the second degree coefficient in the spherical harmonic expansion of the gravitational

field. For an ellipsoid with a severe flattening of 2/3, J_2 reaches 0.25 and the correction to the mass is on the order of 4%.

22. Radar astrometry was published in MPEC 2001-Q33.
23. The large uncertainty is due primarily to the 60% relative uncertainty on volume (three times the relative uncertainty on the radius of the primary). The application of shape-modeling techniques (15) is expected to improve the size estimate and to reduce those error bars considerably.
24. G. J. Consolmagno, D. T. Britt, *Meteorit. Planet. Sci.* **33**, 1231 (1998).
25. J. Veverka *et al.*, *Icarus*, **140**, 3 (1999).
26. The height at which an orbiting secondary has a revolution period equal to the spin period of the primary is called the synchronous height. It is only a few meters above the surface of the primary in this case.
27. The tidal torque and rate of change in a are proportional to the k_2 Love number of the primary, i.e., its response coefficient to a centrifugal potential, and are inversely proportional to the tidal dissipation factor Q (52):

$$\dot{a} = 3\frac{k_2}{Q}\frac{M_s}{M_p}\left(\frac{R_p}{a}\right)^5 na \quad (2)$$

where M_s and M_p are the masses of the secondary and primary, respectively, and other quantities have been defined in the text. Solving for k_2/Q after integration,

$$\frac{k_2}{Q} = \frac{2}{39}\frac{M_p}{M_s}\left(\frac{a}{R_p}\right)^5\frac{1}{nT} \quad (3)$$

where T is the time scale for orbital evolution. This ratio is related to material properties through $k_2 = [(3/2)/(1+\tilde{\mu})]$ and $\tilde{\mu} = 19\mu/2\rho g R_p$, where g is the surface gravity, μ is the rigidity or shear modulus, and $\tilde{\mu}$ is the effective rigidity or ratio of elastic and gravitational forces.
28. B. J. Gladman *et al.*, *Science* **277**, 197 (1997).
29. P. Goldreich, S. Soter, *Icarus* **5**, 375 (1966).
30. The tidal despinning time scale is given by

$$\tau = \frac{4}{15}\frac{Q}{k_2}\frac{M_s}{M_p^2}\frac{a^6}{R_s^3}\frac{\Delta\omega}{G} \quad (4)$$

where $\Delta\omega$ is the change in spin rate (52).
31. Although the specific binding energy of this system is less than 0.01 J, it can probably survive gentle orbital perturbations that act on time scales much longer than the revolution period of the satellite. For instance, drift rates due to the Yarkovsky effect are on the order of 10^{-4} AU/My (53).
32. S. J. Weidenschilling, P. Paolicchi, V. Zappalà, in *Asteroids II*, R. P. Binzel, T. Gehrels, M. S. Matthews, Eds. (Univ. of Arizona Press, Tucson, 1989), p. 643.
33. D. D. Durda, *Icarus* **120**, 212 (1996).
34. T. C. Van Flandern, E. F. Tedesco, R. P. Binzel, in *Asteroids I*, T. Gehrels, Ed. (Univ. of Arizona Press, Tucson, 1979), p. 443.
35. W. K. Hartmann, in *Asteroids I*, T. Gehrels, Ed. (Univ. of Arizona Press, Tucson, 1979), p. 466.
36. S. J. Weidenschilling, *Icarus* **44**, 807 (1980).
37. The breakup rate of a fluid or strengthless body occurs when the synchronous height (26) corresponds to the radius of the object itself. The critical rotation period expressed in hours is $P_{crit} = 3.3/\sqrt{\rho}$, or 2.5 hours for the nominal density of 2000 DP107.
38. W. F. Bottke Jr., H. J. Melosh, *Nature* **381**, 51 (1996).
39. E. Asphaug, W. Benz, *Icarus* **121**, 225 (1996).
40. D. C. Richardson, W. F. Bottke Jr., S. G. Love, *Icarus* **134**, 47 (1998).
41. S. Sridhar, S. Tremaine, *Icarus* **95**, 86 (1992).
42. The Roche limit is the semimajor axis within which a prograde and strengthless satellite is disrupted by planetary tidal forces. It is given by $R_{roche} = 2.45R_p(\rho_p/\rho_s)^{1/3}$, where ρ_p and ρ_s are the densities of the planet and satellite, respectively.
43. Because the system's total angular momentum is conserved during orbital expansion, the spin angular momentum must decrease whereas the orbital momentum increases. [In the Earth-Moon system, this process accounts for the lengthening of the day at a rate of ~1.6 ms/cy and the recession of the Moon at a rate of ~3.8 m/cy (52).] Conversely, if the secondary formed near the primary, the primary's spin

angular momentum must have been larger at the time of formation by an amount equal to the current orbital angular momentum.
44. The primary of 2000 DP107 spins at a rate close to the maximum rate that a strengthless body of density 1.7 g cm^{-3} can sustain without disruption (37). The addition of the orbital angular momentum, ~6.7×10^{12} kg m^2 s^{-1}, to the primary's spin angular momentum, ~1.8×10^{13} kg m^2 s^{-1}, would result in a 2-hour spin period at the time of formation, which is below the critical period to avoid breakup (37).
45. Pravec and Harris (6) do not observe spin periods smaller than 2.2 hours in the sample of asteroids larger than 200 m. They interpret the sharp truncation in spin rates as evidence that most asteroids larger than a few hundred meters in size are gravitationally bound aggregates. Because such aggregates are more prone to tidal fission than monolithic bodies, this notion and the observed size threshold are consistent with the formation of asteroid binaries by tidal disruption.
46. W. J. Merline *et al.*, *Nature* **401**, 565 (1999).
47. W. J. Merline *et al.*, IAU Circ. No. 7503 (2000).
48. W. J. Merline *et al.*, IAU Circ. No. 7827 (2002).
49. M. E. Brown, J. L. Margot, IAU Circ. No. 7588 (2001).
50. J. L. Margot, M. E. Brown, IAU Circ. No. 7703 (2001).
51. R. Greenberg, *Astron. J.* **86**, 912 (1981).
52. S. J. Peale, *Annu. Rev. Astron. Astrophys.* **37**, 533 (1999).
53. P. Farinella, D. Vokrouhlický, W. K. Hartmann, *Icarus* **132**, 378 (1998).
54. There is a fundamental inclination ambiguity in the determination of orbits from range-Doppler data obtained with poor orientational coverage. Observations over a range of aspect angles can overcome this ambiguity. By combining the Goldstone and Arecibo data, the angular leverage for 2000 DP107 corre-

sponds to 40° of sky motion. The detection of occultations in the radar data or of occultations or eclipses in the lightcurve data can also place strong constraints on the inclination of the orbit. In general, a combination of radar and lightcurve observations will yield the best orbital determinations.
55. To test the robustness of our solution against measurement errors, we generated 99 synthetic data sets by adding random noise to our measurements, with the standard deviation of the noise corresponding to our measurement uncertainties scaled by the square root of reduced χ^2. Each synthetic data set underwent the same minimization procedure as the actual data. We find that most solutions fall within our quoted uncertainties, with the exception of pathologic solutions in narrow valleys of the χ^2 space. The pathologic solutions have large semimajor axes and orbital inclinations with respect to the line-of-sight (54). They can be discarded because their geometry does not allow for occultation or eclipse events reported from lightcurve observations (18).
56. We thank P. Nicholson, P. Goldreich, W. Bottke, and E. Asphaug for fruitful discussions on tidal deformation and evolution, and the staffs at Goldstone and Arecibo for assistance with the observations. J.L.M. thanks S. Kulkarni for financial support. The Arecibo Observatory is part of the National Astronomy and Ionosphere Center, which is operated by Cornell University under a cooperative agreement with the National Science Foundation and with support from NASA. This work was supported in part by the Jet Propulsion Laboratory, operated by the California Institute of Technology under contract with NASA.

Metasomatic Origin of Quartz-Pyroxene Rock, Akilia, Greenland, and Implications for Earth's Earliest Life

Christopher M. Fedo[1]* and Martin J. Whitehouse[2]

A quartz-pyroxene rock interpreted as a banded iron formation (BIF) from the island of Akilia, southwest Greenland, contains ^{13}C-depleted graphite that has been claimed as evidence for the oldest (>3850 million years ago) life on Earth. Field relationships on Akilia document multiple intense deformation events that have resulted in parallel transposition of Early Archean rocks and significant boudinage, the tails of which commonly form the banding in the quartz-pyroxene rock. Geochemical data possess distinct characteristics consistent with an ultramafic igneous, not BIF, protolith for this lithology and the adjacent schists. Later metasomatic silica and iron introduction have merely resulted in a rock that superficially resembles a BIF. An ultramafic igneous origin invalidates claims that the carbon isotopic composition of graphite inclusions represents evidence for life at the time of crystallization.

On the island of Akilia, outer Gothåbsfjord, southwest Greenland (Fig. 1, A and B), a sequence of lithologies that has been interpreted as mafic volcanic rocks intercalated with silicious sedimentary rocks chemically precipitated from seawater [banded iron formation (BIF)] contains carbon isotopic signatures that have been interpreted as perhaps the oldest known life on Earth [>3850 million years ago (Ma)] (1–3), overlapping in age with potentially planet-sterilizing asteroid impacts (4, 5). Here we present new geologic, petrologic, and geochemical evidence that favors a metasomatized ultramafic

[1]Department of Earth and Environmental Sciences, George Washington University, Washington, DC 20052, USA. [2]Swedish Museum of Natural History, Laboratory for Isotope Geology, Box 50007, SE-104 05 Stockholm, Sweden.

*To whom correspondence should be addressed. E-mail: cfedo@gwu.edu